

Hydrodynamics of gas–liquid slug flow along vertical pipes in turbulent regime—An experimental study

T.S. Mayor, V. Ferreira, A.M.F.R. Pinto, J.B.L.M. Campos *

Centro de Estudos de Fenómenos de Transporte, Departamento de Engenharia Química, Faculdade de Engenharia da Universidade do Porto, Rua Dr. Roberto Frias 4200-465 Porto, Portugal

ARTICLE INFO

Article history:

Received 27 December 2006

Received in revised form 13 February 2008

Accepted 27 February 2008

Available online 23 April 2008

Keywords:

Two-phase flow

Slug flow

Bubble columns

Flow visualization

Image analysis

Bubble length

ABSTRACT

An experimental study on free-bubbling gas–liquid (air–water) vertical slug flow was developed using a non-intrusive image analysis technique. The flow pattern in the near-wake of the bubbles and in the main liquid between bubbles was turbulent. A single correlation for the bubble-to-bubble interaction is proposed, relating the trailing bubble velocity to the length of the liquid slug ahead of the bubble. The proposed correlation is shown to be independent of column diameter, column vertical coordinate, superficial liquid and gas velocities and the velocity and length of the leading bubble. Frequency distribution curves, averages, modes and standard deviations are reported, for distributions of bubble velocity, bubble length and liquid slug length, for each experimental condition studied. Good agreement was found between theoretical predictions and experimental results regarding the upward velocity of undisturbed bubbles, in a 0.032 m internal diameter column. A considerable discrepancy was found, though, for a 0.052 m internal diameter column. The acquired experimental data are crucial for the development and validation of a robust slug flow simulator.

© 2008 Elsevier Inc. All rights reserved.

1. Introduction

Slug flow is a highly intermittent and irregular two-phase flow regime observed when gas and liquid flow simultaneously in a pipe, over certain ranges of gas and liquid flow rates. The slug flow pattern is characterised by elongated bullet-shaped gas bubbles, known as Taylor bubbles, separated by liquid slugs which often contain small dispersed bubbles. These long bubbles occupy most of the cross sectional area of the pipe, forcing the liquid to flow around them, in the opposite direction, in a very thin film where the shear forces tend to balance the body forces (in a free-falling liquid film). At the rear of the bubble, the liquid film expands, creating a separate flow – the bubble wake. Depending on the flow parameters and the liquid physical properties, the flow in the bubble wake varies from a well-defined recirculation flow (laminar wake) to a turbulent one where small and random recirculation regions can be observed (turbulent wake). In both situations, the liquid in the wake flows upwards at a mean velocity equal to the bubble velocity, thus travelling attached to the rear of the bubble. Below the bubble wake (in a reference frame moving with the bubble) the liquid starts evolving to the undisturbed flow pattern. Interesting contributions on the flow field characterization at the

near bubble wake region have been given, for instance, by Van Hout et al. (2002a) or Sotiriadis and Thorpe (2005).

The undisturbed velocity of Taylor bubbles, U_B , has been studied extensively (Nicklin et al., 1962; Collins et al., 1978, among others) and it is generally assumed to be expressed by the sum of the drift velocity (the velocity of the bubble in stagnant liquid, U_∞) and a local contribution of the maximum velocity of the liquid flowing ahead of the bubble nose:

$$U_B = U_\infty + C(U_L + U_G) \quad (1)$$

where U_L is the superficial liquid velocity, U_G the superficial gas velocity and C a parameter ranging from approximately 1.2, for fully developed turbulent liquid flow, to 2.0, for laminar liquid flow. For inertia controlled regime (range according to White and Beardmore, 1962) the drift velocity is given by:

$$U_\infty = 0.35\sqrt{gD} \quad (2)$$

where g and D are the acceleration of gravity and the column internal diameter, respectively.

When a Taylor bubble flows in the wake of a leading bubble or in the disturbed liquid below it, its velocity tends to increase until it eventually merges with the leading bubble. After the merging process, the bubble length increases. Several authors (Moissis and Griffith, 1962; Pinto and Campos, 1996; Pinto et al., 1998; Aladjem Talvy et al., 2000; Van Hout et al., 2001, 2002b) refer to a minimum liquid slug length for having a stabilized slug flow

* Corresponding author. Tel.: +351 225081692; fax: +351 225081449.
E-mail address: jmc@fe.up.pt (J.B.L.M. Campos).

Nomenclature

a, b, c	dimensionless fit parameters [–]
C	empirical coefficient [–]
D	column internal diameter [m]
g	acceleration of gravity [m s^{-2}]
$h_{\text{b}, i}$	length of gas bubble i [m]
$h_{\text{cal.}, \text{m}}$	height of the calibration element, in metres [m]
$h_{\text{cal.}, \text{px}}$	height of the calibration element, in pixels [pixel]
H_{cam}	vertical coordinate of the video camera (from the base of the column) [m]
h_{im}	height of the field of view [m]
h_s	length of liquid slug [m]
$h_{s,i}$	length of liquid slug i [m]
n	number of element in each class [#]
S_x	sample standard deviation (for bubble velocity) [m/s]
t	critical value (t -student distribution) [–]
t_j	time instant [s]
t_{j+1}	time instant immediately after t_j [s]
U_∞	upward bubble velocity in a stagnant liquid (drift velocity) [m/s]
U_B	upward bubble velocity [m/s]
U_B^{exp}	experimental average upward bubble velocity in undisturbed conditions [m/s]
U_G	superficial gas velocity [m/s]

U_i	upward velocity of bubble i (U_i^{trail} and U_i^{lead} for trailing and leading bubble, respectively) [m/s]
U_L	superficial liquid velocity [m/s]
U_M	superficial mixture velocity ($= U_L + U_L$) [m/s]
V_s	liquid slug velocity relative to the bubble ($= U_B^{\text{exp}} - U_M$) [m/s]
$z_{\text{nose}, i}$	vertical coordinate of the nose of bubble i , within each image frame [pixel]
$z_{\text{rear}, i}$	vertical coordinate of the rear of bubble i , within each image frame [pixel]

Dimensionless groups

Re_{U_M}	Reynolds number based on the mixture velocity ($= \rho U_M D / \mu$)
Re_{V_s}	Reynolds number based on the liquid slug velocity relative to the bubble ($= \rho V_s D / \mu$)

Greek symbols

σ	standard deviation of the distribution of bubble velocities [m/s]
μ	liquid viscosity [Pa s]
ρ	liquid density [kg m^{-3}]

pattern. They have suggested empirical correlations relating the velocity of a trailing bubble i , U_i^{trail} , with the separation distance between consecutive bubbles, h_s . Pinto and Campos, 1996; Pinto et al., 1998; Aladjem Talvy et al., 2000 reported correlations supported in data from controlled bubble injection experiments, while Van Hout et al., 2001 provided a correlation supported by data from naturally occurring continuous gas–liquid slug flow experiments:

$$\frac{U_i^{\text{trail}}}{U_B} = a + b e^{-ch_s/D} + \frac{1}{h_s/D} \quad (3)$$

where U_B is the upward bubble velocity as defined by Eq. (1), and a , b and c are fitting parameters. However, further investigation is necessary to assess the dependence of these parameters on gas and liquid flow rates and liquid regimes. Additionally, some discrepancies are reported between the undisturbed bubble velocities observed and theoretical predictions (Eq. (1) with $C = 1.2$) for the larger column diameter (0.054 m). The occurrence of highly distorted bubbles (observed along the rise) and highly aerated liquid slugs are suggested to account for these discrepancies. More recently, Van Hout et al., 2002b reported a study in which the same technique (based on optical fibre probes) was applied together with an image processing technique, in order to investigate the hydrodynamics of elongated bubbles in continuous slug flow. The non-intrusive image processing approach was applied in continuous slug flow conditions to a small sample of elongated bubbles (30–40).

The dynamic and complex behaviour of Taylor bubbles creates some difficulties in the development of predictive algorithms capable of providing information about continuous gas–liquid slug flow. In particular, bubble and slug length distributions, bubble velocity distribution, gas entrainment, coalescence rate and minimum pipe length for stabilised flow patterns are all crucial data for the optimal design of slug flow applications.

The main goal of the present work is to acquire more experimental data on free-bubbling gas–liquid slug flow, in order to formulate a predictive model. Hydrodynamics and statistical parameters were obtained using a non-intrusive experimental technique (based on image analysis) in two pipe diameters, for sev-

eral gas and liquid flow rates and in two positions along the pipe. Several hundreds of elongated bubbles (1200–1500) were analysed for each experimental condition. These data allow the analysis of the role played by the gas and liquid flow rates and by the velocity and length of the leading bubble, over the dependence of the trailing bubble velocity on the length of the liquid slug flowing ahead of it. An empirical bubble-to-bubble interaction correlation is proposed. Experimental values for parameter C and drift velocity are analysed and compared with the values in the literature. The experimental data are compared with the findings of other researchers and supports a predictive model used in a slug flow simulator (Mayor et al., 2007a).

2. Experimental set-up

The experimental apparatus is shown schematically in Fig. 1. Experiments were performed in acrylic vertical pipes 6.5 m long with internal diameters of 0.032 m and 0.052 m. Tap water was used as flowing medium at superficial velocities up to 0.30 m/s.

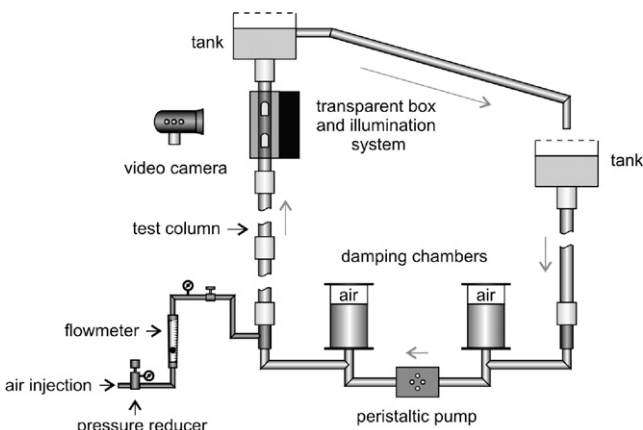


Fig. 1. Experimental set-up.

The flow was set and controlled by a peristaltic pump with damping chambers placed at the pump inlet and outlet to assure a continuous flow. A large open tank with a lateral outlet was mounted at the top of the pipe to minimise free-surface oscillations (more details on this issue can be found in Mayor et al., 2008). The liquid flow rate was measured at the outlet of the tank, before and after each experiment. The liquid temperature was measured by a thermocouple placed inside the tank. Air from a pressure line was introduced laterally at the base of the column through a 3 mm internal diameter injector. The air flow rate was measured by calibrated rotameters at superficial velocities up to 0.30 m/s (at 1 bar and 20 °C).

Images of slug flow were recorded using a Canon digital video camcorder (model XM1) in two pipe sections comprising the vertical positions 3.25 m and 5.40 m (measured from the base of the column). A rectangular transparent acrylic box filled with water was fitted to the pipe at the measuring sections, in order to reduce image distortion and heating effects from the light source.

The digital video camcorder operated at a frequency of 25 Hz and the exposure times varied from 1/4000 s to 1/8000 s. A 90° rotation of the camera was chosen for better pixel resolution in the vertical coordinate (non-rotated camera field of view is 720 (width) × 576 (height) pixels). Different camera focal lengths were used according to the flow complexity and the average bubble and liquid slug dimensions, resulting in up to 0.6 m of pipe captured in the camera field of view.

3. Image processing

The recorded videos were transferred to a personal computer hard drive using video editing software (Adobe Premiere).

Stripes containing the test column were extracted from the original videos and further processed using a MATLAB code (The MathWorks, 2002) specially developed for this purpose. Each video file was loaded into MATLAB as a sequence of frames (a frame at each 0.04 s, corresponding to a frequency of 25 Hz). A sequential procedure was then implemented to process each image frame, the outcome of which is shown in Fig. 2.

Bubble boundary definition is difficult due to the existence of more or less aerated liquid slugs (Fig. 2a). Thus, a minimum bubble length was defined in order to distinguish between Taylor bubbles and small bubbles in the liquid slug. Depending on the flow complexity and average bubble length, a threshold length between 1D and 3D was used throughout the analysis of all experiments.

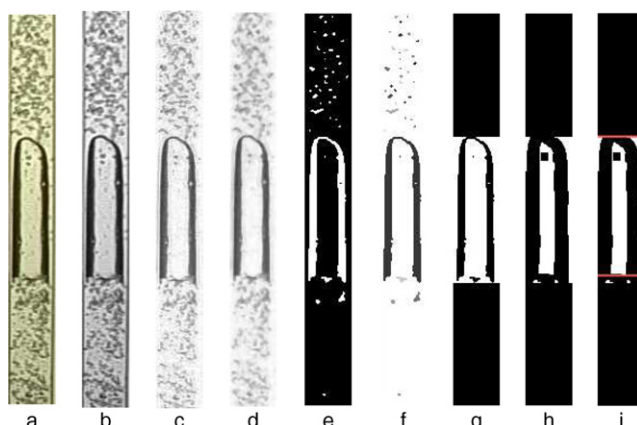


Fig. 2. Sequential steps in the image process ($U_L \approx 0.10 \text{ m/s}$, $U_G \approx 0.10 \text{ m/s}$, $D = 0.032 \text{ m}$): a – RGB image; b – grayscale image; c – after background subtraction; d – after median filter; e – after conversion to binary mode; f – after labelling; g – after object analysis; h – after erosion and i – bubble boundaries.

The use of object length as a sorting parameter allowed immediate definition of the Taylor bubble nose as well as a rough estimate of the position of the Taylor bubble rear. This uncertainty is due to oscillations in the bubble rear as Taylor bubbles flow in the column, and to the small bubbles travelling in the liquid wake. Moreover, as stressed by Nogueira et al. (2003), bubble bottom conformation may also be an issue while defining the positioning of bubble rear (in particular for viscous solutions). These difficulties were lessened by implementing an image erosion procedure to isolate the central white area of each bubble (Fig. 2h), a region whose lowest white pixel matches the beginning of the bubble wake region (Fig. 2i). Thus, this strategy allowed for the determination of robust estimates of bubble length (discarding the wake region).

4. The data analysis from image processing

The image processing procedure (Mayor et al., 2007b) was implemented on every video frame. This permitted to gather information about the presence, positioning and dimension of bubbles, in the video frames. Furthermore, by analysing the characteristics of the bubbles (i.e. length and distance) and their displacements (i.e. velocity) along the column, it is possible to compile information about the flow pattern characteristics, for every experimental condition. Two different studies were performed: one describing the flow pattern at a fixed column position (fixed-point data analysis), and another focussing on the bubble-to-bubble interac-

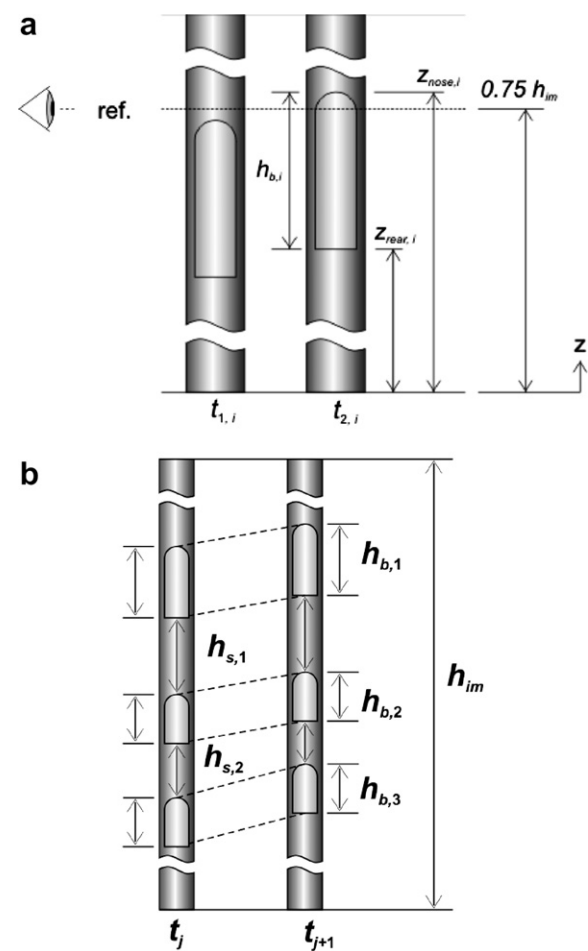


Fig. 3. Representation of the camera field of view in: (a) fixed-point analysis and (b) moving-point analysis.

tion as bubbles move along the column (moving-point data analysis).

4.1. Fixed-point data analysis

Fig. 3a depicts the camera's field of view in a slug flow experiment. An imaginary reference line corresponding to 75% of the field of view height was drawn. Bubbles are recognized when their noses cross the reference line.

The bubble velocity, U_b , is given by $(z_{\text{nose},i}^{t_{2,i}} - z_{\text{nose},i}^{t_{1,i}})/(t_{2,i} - t_{1,i})$, where $z_{\text{nose},i}$ refers to the vertical coordinate of the bubble nose and $t_{1,i}$ and $t_{2,i}$ represent consecutive instants.

The bubble length is obtained directly from the position of its boundaries ($h_{b,i} = z_{\text{nose},i}^{t_{2,i}} - z_{\text{rear},i}^{t_{2,i}}$) whereas the liquid slug length ahead of bubble i is computed from the coordinate of the rear of the previous bubble (bubble $i - 1$) and the coordinate of the nose of bubble i ($h_{s,i-1} = z_{\text{rear},i-1}^{t_{2,i}} - z_{\text{nose},i}^{t_{2,i}}$). The coordinate of the rear of bubble $i - 1$, at instant $t_{2,i}$, can be predicted by $z_{\text{rear},i-1}^{t_{2,i}} = z_{\text{nose},i-1}^{t_{2,i-1}} + (t_{2,i} - t_{2,i-1})U_{i-1}^{t_{2,i-1}} - h_{b,i-1}$. The variable $t_{2,i-1}$ refers to the instant at which the nose of bubble $i - 1$ crossed the reference line. In the above prediction it is assumed that bubble $i - 1$ has constant upward velocity between instants $t_{2,i-1}$ and $t_{2,i}$. This assumption is reasonable unless the bubble is coalescing, interacting or instantly accelerating or decelerating by the time it passes the reference line. In that case, and as a result of the aforementioned assumption, a marginal increase in the occurrence of extreme values of slug length (either short or long) might take place. Despite this fact, no major effect of this assumption is expected for the most probable value and average for the slug length variable (due to compensation).

The above procedure was implemented for each video frame to gather information about every bubble (bubble length, velocity and liquid slug length). These variables have pixel units (or pixel/s in the velocity case). To accomplish their conversion to real length units, the following correction must be computed:

$$\text{Variable [m or m/s]} = \text{variable [pixel or pixel/s]} \frac{h_{\text{cal},m}}{h_{\text{cal},px}} \quad (4)$$

where $h_{\text{cal},m}$ and $h_{\text{cal},px}$ refer to the height of the calibration element in metres and pixels units, respectively.

4.2. Moving-point data analysis

In the moving-point data analysis, the focus is put on bubble-to-bubble interaction. Hence, for higher accuracy, it is important to use an image magnification in which more than one Taylor bubble is visible in the camera field of view. In this scenario, the relation between bubble velocity and liquid slug length ahead of the bubble is obtained without using predictions to compute bubble boundary positioning as in the previous section. Fig. 3b depicts this situation.

Consecutive instants t_j and t_{j+1} are chosen considering the requirement of frames with equal number of bubbles, and with all bubble boundaries inside the camera field of view (no bubbles entering or exiting the field of view).

Bubble velocities U_i are calculated using $(z_{\text{nose},i}^{t_{j+1}} - z_{\text{nose},i}^{t_j})/(t_{j+1} - t_j)$ for every bubble in the chosen frames. Bubble and liquid slug lengths are computed using $z_{\text{nose},i} - z_{\text{rear},i}$ and $z_{\text{rear},i-1} - z_{\text{nose},i}$, respectively. Notice that, for n bubbles in a frame, only $n - 1$ liquid slugs are computed. Additionally, the last two equations are applied to each pair of consecutive frames and, therefore, average values for each bubble and liquid slug length are calculated (from every two consecutive frames).

As referred to in the previous section, a correction must be computed to convert the aforementioned variables to real length (or velocity) units (see Eq. (4)). An error analysis of the main flow parameters has been performed, the main results of which are shown in brief in Appendix.

5. Experimental data

Several parameters were measured during the analysis of the slug flow experiments in co-current conditions. The flow pattern in the main liquid between bubbles and in the wake of the bubbles was turbulent (Reynolds number in the main liquid in the range 4120–18,740, based on the mixture velocity, U_M ($= U_G + U_L$); Reynolds number in the wake in the range 6230–25,830, based on the liquid slug velocity relative to the bubble, V_S ($= U_B^{\text{exp}} - U_M$)); turbulent regime in the wake is acknowledged for Reynolds numbers higher than 525, according to Pinto et al., 1998. The liquid slug velocity relative to the bubble was used as the characteristic velocity based on previous studies, such as those of Pinto et al., 1998 and Nogueira et al., 2006. However, other researchers, e.g. Shemer et al., 2007, employed also the bubble velocity as the characteristic velocity).

The main parameters obtained through fixed-point analysis are the distributions of the bubble velocity, bubble length and liquid slug length, and the corresponding average values. Additionally, the experimental average upward bubble velocity, U_B^{exp} , in undisturbed conditions, is also worthy of interest, since it is used in the normalization procedures described later. Notice that according to the analysis of the slug flow data, only bubbles flowing after long slugs ($h_s \geq 8-10D$) are considered undisturbed. Experimental values of parameter C and drift velocity are determined for both columns tested.

The main output of the moving-point analysis is the bubble-to-bubble interaction curve, relating the velocity of the trailing bubble, normalized by U_B^{exp} , to the liquid slug length ahead of the bubble (h_s).

Depending on flow conditions, 1200–1500 bubbles were processed by the fixed-point data analysis (distribution curves and corresponding averages), and several thousand frames with more than one bubble were considered in the moving-point data analysis (bubble-to-bubble interaction curve). 500–1000 bubbles were taken into account in the calculation of the experimental average upward bubble velocities in undisturbed conditions (U_B^{exp}).

5.1. Reproducibility of the method and representativity of the samples

In order to assess the reproducibility of the image analysis method, three independent experiments with equal superficial liquid and gas velocities ($U_L \approx 0.10 \text{ m/s}$, $U_G \approx 0.085 \text{ m/s}$, $D = 0.032 \text{ m}$) were compared. This comparison focussed on the bubble-to-bubble interaction curve, on the frequency distribution curves and on the corresponding average values for several parameters: bubble velocity (U), bubble length (h_b) and liquid slug length (h_s). Fig. 4a shows this comparison regarding the bubble-to-bubble interaction curve.

The velocities of leading and trailing bubbles (U_i^{lead} and U_i^{trail}), normalized by the experimental average upward bubble velocity in undisturbed conditions (U_B^{exp}), are plotted as a function of their separation distance (h_s or liquid slug length). These results show that the image analysis method, used as a tool to study the slug flow pattern, has considerable reproducibility. Similar conclusions are drawn when focusing on the frequency distribution curves of U , h_b and h_s as well as on the corresponding average values.

In order to evaluate the minimal sample size needed to obtain significant values of the parameters under study, three samples consisting of 500, 1000 and 1500 bubbles were drawn from a general population of 2000 bubbles (as before, $U_L \approx 0.10 \text{ m/s}$, $U_G \approx 0.085 \text{ m/s}$, $D = 0.032 \text{ m}$). The frequency distribution curves of liquid slug length are shown in Fig. 4b (for a bin size of 1.5D). From this chart it can be concluded that a sample size of 1000 elements assures adequate representation of the parent population.

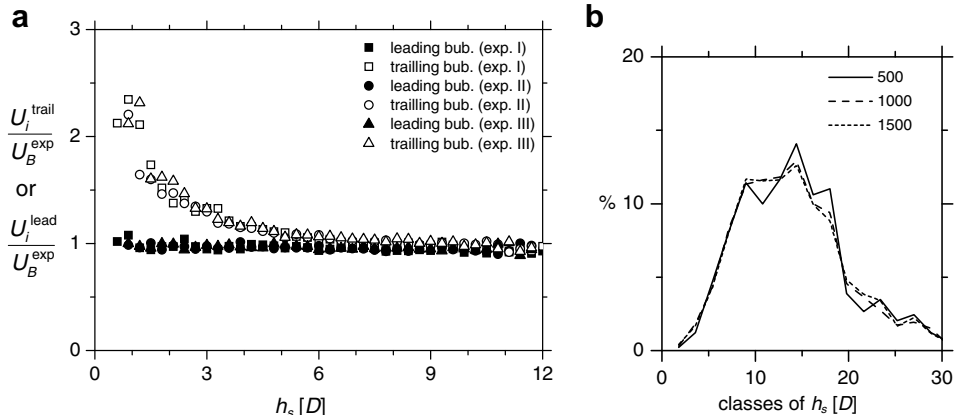


Fig. 4. (a) bubble-to-bubble interaction curve for three similar experiments and (b) slug length frequency distribution curves for samples with 500, 1000 and 1500 bubbles; $U_L \approx 0.10 \text{ m/s}$ and $U_G \approx 0.085 \text{ m/s}$; vertical coordinate: 5.4 m; column diameter: 0.032 m.

This is based on the reduced changes in the frequency distribution curves for larger samples (for liquid slug length, bubble length and bubble velocity). Nevertheless, a minimum sample size requirement of 1200 bubbles was set for all experiments, for increased representativity.

5.2. A systematic study of the bubble-to-bubble interaction curve

Several experimental conditions were studied in order to evaluate the universality of the bubble-to-bubble interaction curve (for turbulent regime). In particular, focus was put on the influence of parameters such as the vertical column coordinate, the superficial liquid and gas velocities, the velocity and length of the leading bubble and the column diameter.

5.2.1. Vertical column position and column diameter

In order to check the universality of the interaction curve along the column, two similar experiments are compared, at different vertical column coordinates (3.25 m and 5.40 m), for the 0.032 m internal diameter column. Superficial liquid and gas velocities are 0.045 m/s and 0.085 m/s, respectively. The superficial gas velocity is at ambient pressure. This reference pressure is used for all gas flow data mentioned in this document, unless stated otherwise. Fig. 5a shows the curve of velocity ratios ($U_i^{\text{trail}}/U_B^{\text{exp}}$ and $U_i^{\text{lead}}/U_B^{\text{exp}}$) plotted against the normalized liquid slug length (h_s).

Acceleration of the trailing bubble towards the leading one occurs at both column coordinates for liquid slugs shorter than

8–10D. Indeed, the entire bubble-to-bubble interaction curve is similar for the two experiments, indicating its independence from the column vertical coordinate. Additionally, the chart above shows that any eventual influence of the initial bubble and slug distributions (“entrance effects”), over the slug flow pattern, is already unperceived at coordinate 3.25 m.

As referred to in Section 4.2, for greater accuracy, the moving-point data analysis requires that more than one Taylor bubble is visible in the camera field of view. Since only one video camera was used, this can only be achieved by increasing the distance between the video camera and the test section (i.e. by zooming the image out, with consequent loss in resolution) a balance must be found between image magnification and image resolution. A balance was established for an image magnification covering the movement of two bubbles, at the maximum distance of 11–12D. Considering that the bubble-to-bubble interaction occurs over shorter distances (8–10D) no limitation is introduced in the analysis by this image magnification/resolution compromise. Notice that, for greater curve smoothness, the velocity ratios are gathered and averaged according to the liquid slug length class (classes of 0.3D). Moreover, this averaging approach is used in all the interaction curves presented.

In order to check the validity of the interaction curve for different column diameters, two experiments with similar superficial gas and liquid velocity ($U_L \approx 0.15 \text{ m/s}$, $U_G \approx 0.10 \text{ m/s}$) were performed in columns with internal diameters equal to 0.032 m and 0.052 m (data were acquired at 5.4 m from the column base).

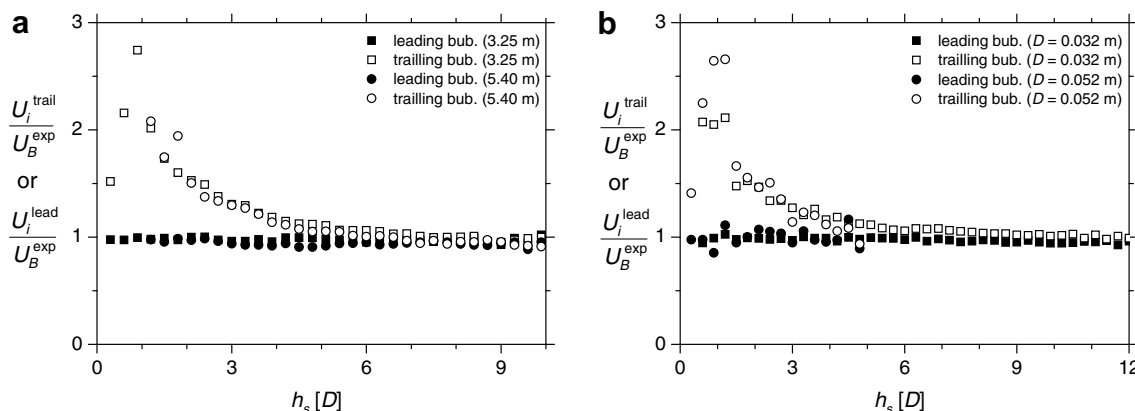


Fig. 5. Bubble-to-bubble interaction curves: (a) at column vertical coordinates 3.25 m and 5.40 m ($U_L \approx 0.045 \text{ m/s}$, $U_G \approx 0.085 \text{ m/s}$, $D = 0.032 \text{ m}$) and (b) for columns with 0.032 m and 0.052 m of internal diameter ($U_L \approx 0.15 \text{ m/s}$, $U_G \approx 0.10 \text{ m/s}$, respectively; vertical coordinate: 5.4 m).

Fig. 5b shows the curve of velocity ratios plotted against the normalized liquid slug length (h_s). This chart indicates that the bubble-to-bubble interaction curve is similar for both column diameters. Notice that, as a consequence of the two bubbles per frame requirement, different column heights (in normalized form) were captured in the camera field of view (5–6D for the 0.052 m column and 11–12D for the 0.032 m column). Despite this fact, the aforementioned interaction similarity is clearly perceived. Higher standard deviations are observed for the larger column, due to the higher aeration of the liquid slugs and to the higher turbulence level of the flow (see Reynolds numbers in Tables 1 and 2 for relevant operating conditions).

5.2.2. Superficial liquid and gas velocity (U_L and U_G)

In Fig. 6a, four experiments with increasing superficial liquid velocity are compared ($U_L \approx 0.045, 0.10, 0.15$ and 0.21 m/s), for constant superficial gas velocity ($U_G \approx 0.085$ m/s). Fig. 6b regards two experiments with increasing superficial gas velocity ($U_G \approx 0.084$ m/s and 0.15 m/s) and constant superficial liquid velocity ($U_L \approx 0.10$ m/s). The data were acquired in a 0.032 m internal diameter column, at vertical coordinate 3.25 m. It can be seen in these charts that the bubble-to-bubble interaction curve is independent of both the superficial liquid and gas velocities.

5.2.3. Velocity and length of the leading bubble

In order to assess the influence of the leading bubble velocity and length over the bubble-to-bubble interaction curve, the data from an experiment ($U_G \approx 0.085$ m/s and $U_L \approx 0.10$ m/s) were thoroughly analysed. In Fig. 7, two distinct versions of bubble pairs are plotted: one showing data with two different leading bubble velocities (Fig. 7a) and another showing data with diverse leading bubble lengths (Fig. 7b). In order to filter the experimental data (pairs of interacting bubbles), the 50th percentiles, of the distributions of the leading bubble velocities and bubble lengths, were used. A value of $12.5D/s$ (bubble velocity relative to column internal diameter) was used to prepare two bubble pair sub-distributions: one with bubble pairs whose leading bubble velocities were higher than $12.5D/s$, and another consisting of bubble pairs whose leading bubble velocities were lower than $12.5D/s$. Likewise, a value of $2.7D$ was used to prepare two alternative bubble pair sub-distributions: one whose leading bubbles were longer than $2.7D$, and another whose leading bubbles were shorter than $2.7D$.

In Fig. 7a, the different average velocity of the leading bubble, for the two experiments being compared ($13.8D/s$ and $11.7D/s$, or 1.07 and 0.91 , after normalization), are clearly perceived. Despite the difference in the leading bubble velocity, a similar acceleration of the trailing bubble occurs at an identical bubble separation

Table 2

Superficial liquid and gas velocities used in several experiments and corresponding Reynolds numbers (based on U_G at ambient pressure and U_B^{\exp})

D [m]	U_L [m/s]	U_G [m/s]	Reynolds number	
			Liquid	Wake
			Re_{U_M}	Re_{V_s}
0.032	0.044	0.084	4122	8526
0.032	0.098	0.085	5876	8378
0.032	0.151	0.088	7640	7875
0.032	0.194	0.085	8926	7568
0.032	0.102	0.088	6069	7582
0.032	0.102	0.158	8321	7443
0.032	0.102	0.205	9822	7596
0.032	0.102	0.260	11,573	7707
0.052	0.047	0.106	7928	24,226
0.052	0.074	0.105	9298	21,806
0.052	0.101	0.105	10,723	21,920
0.052	0.145	0.105	12,980	19,716
0.052	0.101	0.106	10,762	21,881
0.052	0.101	0.160	13,577	23,852
0.052	0.101	0.211	16,234	25,831
0.052	0.101	0.259	18,736	25,691

distance. Thus, it may be concluded that the interaction curve is unaffected by the velocity of the leading bubble. The chart of Fig. 7b, for bubble pairs with different leading bubble lengths, indicates that the interaction curve is also independent from this parameter.

5.3. Approaching coalescence phenomenon – the bubble-to-bubble interaction curve

As shown in the previous sections, the bubble-to-bubble interaction curve is independent of several flow parameters, for turbulent regime in the liquid and in the bubble wake. Indeed, it is possible to model the interaction between two consecutive bubbles by expressing the normalized trailing bubble velocity as a function of the liquid slug length ahead of it. Fig. 8a represents the bubble-to-bubble interaction curve for several experiments, with superficial liquid and gas velocities as shown in Table 1.

By averaging the normalized velocities represented in Fig. 8a, for each slug length class, the smoother bubble-to-bubble interaction curve shown in Fig. 8b is obtained. Error bands corresponding to a 95% confidence level are also represented in the chart of Fig. 8b. They are defined considering the normalized velocities ($U_i^{\text{trail}}/U_B^{\exp}$ and $U_i^{\text{lead}}/U_B^{\exp}$) in each slug length class, and computed as an interval ($\pm tS_x/\sqrt{n}$) around the average normalized velocity. Notice that there are different samples of normalized velocities for each slug length class considered. Moreover, S_x stands for the sample standard deviation, t refers to the t -student distribution and n is the number of class elements.

Fig. 8b shows that the shorter the liquid slugs, the longer the error bands. This fact is obviously related to the higher standard deviation of the velocity samples as bubbles accelerate towards coalescence.

As mentioned before, the acceleration of the trailing bubble towards the leading bubble occurs for liquid slugs shorter than 8–10D. A strong acceleration is observed for liquid slugs shorter than 3D in particular. Additionally, for very small liquid slug lengths ($h_s < 1D$), a decrease in the trailing bubble velocity is observed. These observations are in agreement with the findings of Aladjem Talvy et al. (2000), Van Hout et al. (2001). Moreover, the decrease in the trailing bubble velocity for very short liquid slugs may be related to the dynamics in the main vortex of the bubble wake region, which extends to around 1–2D (Van Hout et al., 2002a; Sotiriadis and Thorpe, 2005). Additionally, it is worth mentioning that very small oscillations of the trailing bubble velocity were

Table 1

Superficial liquid and gas velocities used in several experiments and corresponding Reynolds numbers (based on U_G at ambient pressure and U_B^{\exp}); internal diameter: 0.032 m

	U_L [m/s]	U_G [m/s]	Reynolds number	
			Liquid	Wake
			Re_{U_M}	Re_{V_s}
a	0.044	0.084	4122	8526
b	0.047	0.084	4169	7386
c	0.047	0.084	4169	7386
d	0.097	0.149	7885	7204
e	0.098	0.085	5876	8378
f	0.100	0.083	5849	7067
g	0.102	0.088	6056	8281
h	0.152	0.084	7525	6916
i	0.208	0.084	9336	6726
j	0.208	0.150	11,452	6233

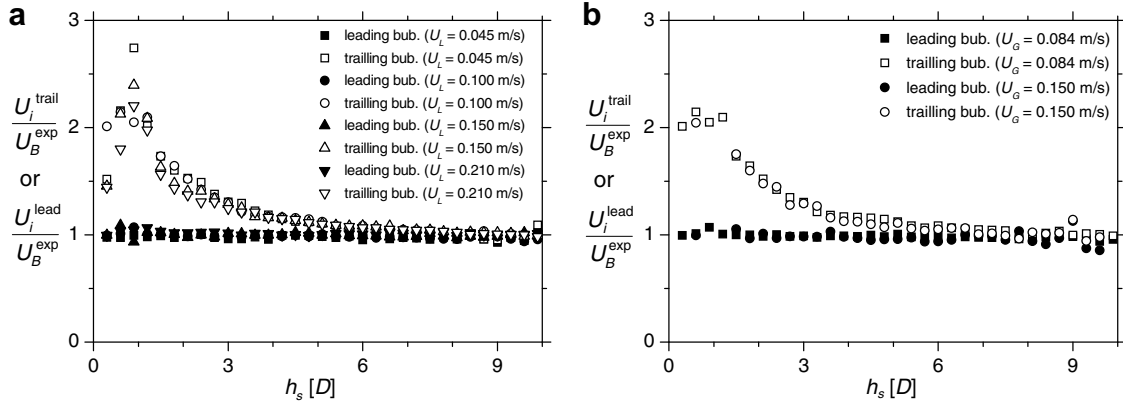


Fig. 6. Bubble-to-bubble interaction curve for: (a) $U_L \approx 0.045, 0.10, 0.15$ and 0.21 m/s ; $U_G \approx 0.085 \text{ m/s}$ and (b) $U_G \approx 0.084 \text{ m/s}$ and 0.15 m/s ; $U_L \approx 0.10 \text{ m/s}$; column diameter: 0.032 m .

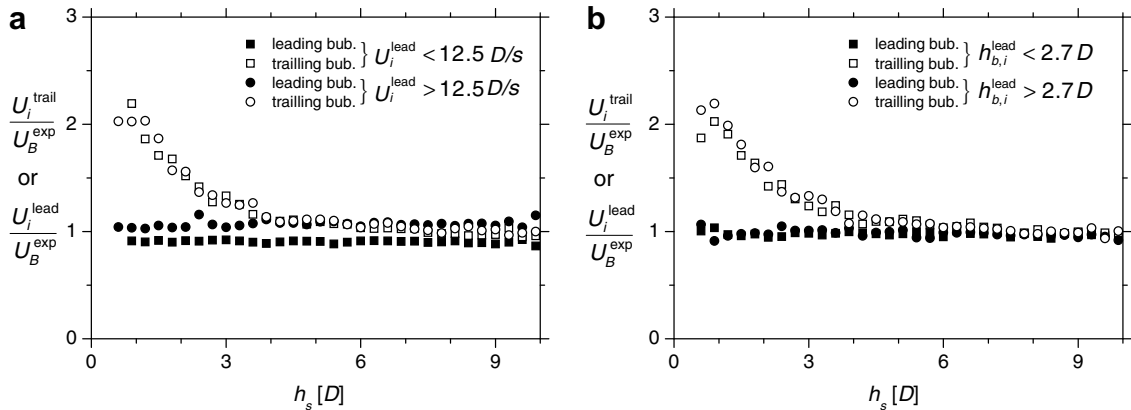


Fig. 7. Bubble-to-bubble interaction curve for experiments with (a) different leading bubble velocity and (b) different leading bubble length; $U_G \approx 0.085$ and $U_L \approx 0.10 \text{ m/s}$; column diameter: 0.032 m .

observed, occasionally, for liquid slugs longer than $10D$, the magnitude of which being smaller than the accuracy of the experimental technique (see [Appendix](#) for more details). These observations are in line with the findings of other researchers (e.g. [Shemer et al., 2007](#)) which also report bubble velocity oscillations for liquid slugs longer than $10D$. Further investigation is, thus, needed to clarify the origin of the aforementioned oscillations (focussing for instance on the eventual influence of the aeration level of the liquid slugs or the slow decay of the leading bubble wake perturbation).

An exponential fit of the trailing bubble velocity data is represented by the full line in [Fig. 8b](#). The corresponding equation is:

$$\frac{U_i^{\text{trail}}}{U_B^{\text{exp}}} = 1 + 2.4e^{-0.8\left(\frac{h_{s,i-1}}{D}\right)^{0.9}} \quad (5)$$

where U_i^{trail} refers to the velocity of the trailing bubble i flowing behind a liquid slug with length h_s , $i - 1$. The bubble velocity is normalized by the experimental average undisturbed bubble velocity (U_B^{exp}). The trailing bubble slowdown for very short liquid slugs was, obviously, discarded in the fitting represented by [Eq. \(5\)](#). Nevertheless, this simplification has negligible effect in terms of simulation as it refers to instants on the verge of coalescence.

In [Fig. 8c](#), the bubble-to-bubble interaction curve obtained is compared with those proposed by [Van Hout et al. \(2001\)](#). These curves are based on data obtained for 0.024 m and 0.054 m internal diameter columns. Despite this fact, and because the corresponding equations differ only on a single parameter (representing the

undisturbed upward bubble velocity), a direct comparison between those curves and the proposed curve can be made. The analysis of the chart shows that, unlike the proposed bubble-to-bubble interaction curve, the models proposed by Van Hout still acknowledge some bubble interaction for liquid slugs longer than $8\text{--}10D$. The present experimental work (0.032 m ID) provided no evidence of such interaction. However, and as mentioned previously, further research efforts are required on this topic.

5.4. Frequency distribution curves and average values of the main flow parameters

The influence of several flow parameters over the frequency distribution curves and corresponding averages is shown, in detail, in the following sections. Focus is put on parameters such as column vertical position, superficial liquid and gas velocities. Two internal diameters are reported (0.032 m and 0.052 m). [Table 2](#) compiles the operating conditions of all experiments reported in this section.

5.4.1. Column I – 0.032 m ID

5.4.1.1. *Flow development along the column.* Two experiments with the same set of superficial liquid and gas velocities are compared in [Figs. 9 and 10](#). Data acquisition occurred at 3.25 and 5.40 m from the column base, in a 0.032 m internal diameter column. The frequency distribution curves (and the corresponding log-normal fits)

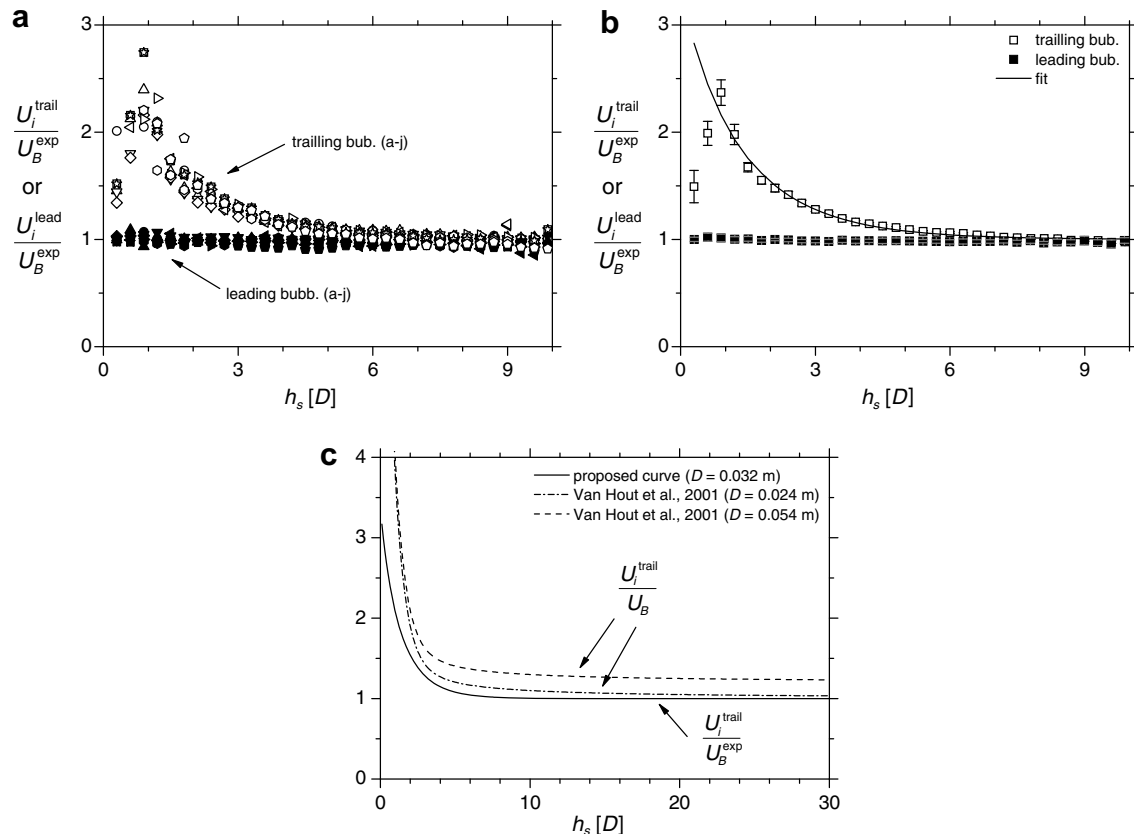


Fig. 8. (a) Bubble-to-bubble interaction curve for several experiments (0.032 m ID); (b) average bubble-to-bubble interaction curve and 95% confidence intervals (0.032 m ID); (c) comparison of the average bubble-to-bubble interaction curve with those proposed by Van Hout et al., 2001, for 0.024 m and 0.054 m ID columns.

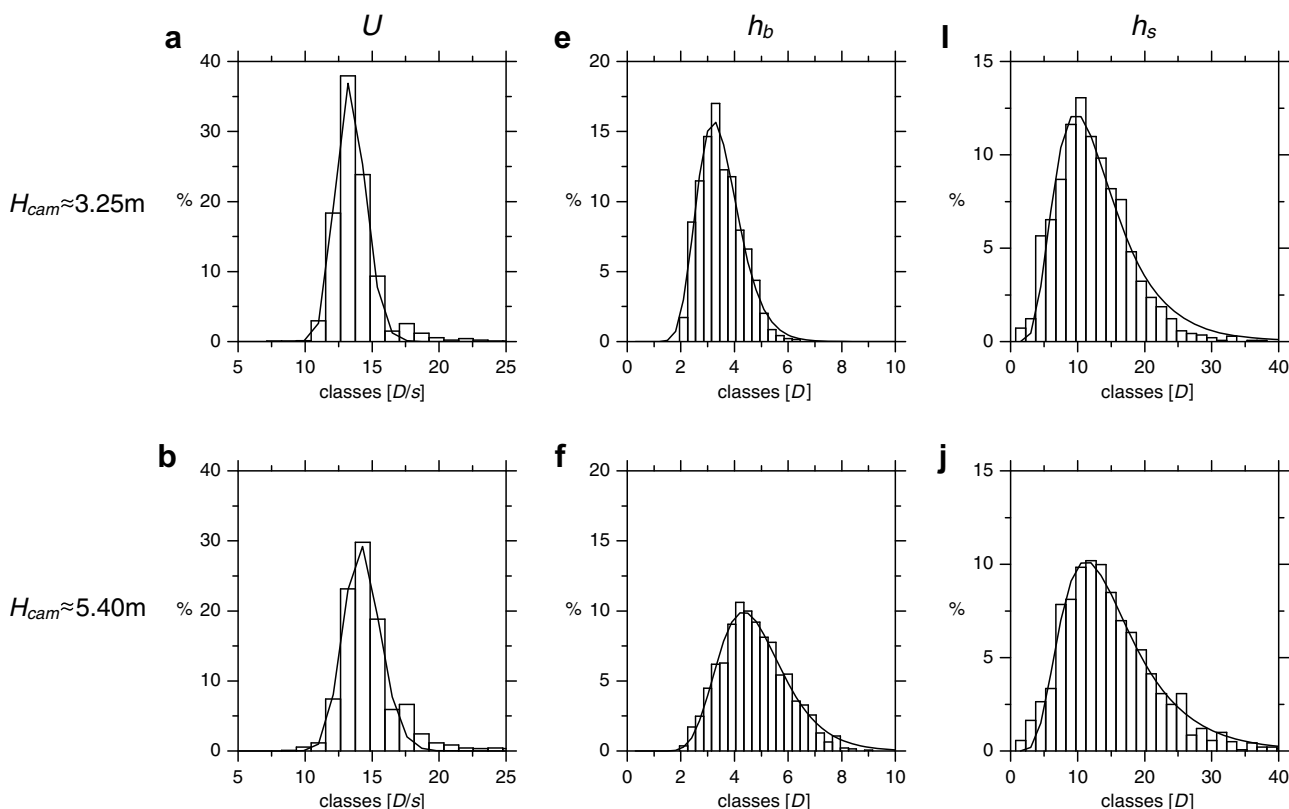


Fig. 9. Frequency distributions curves and log-normal fittings for experiments at 3.25 m and 5.40 m from the column base ($U_L \approx 0.099 \text{ m/s}$, $U_G \approx 0.085 \text{ m/s}$); column diameter: 0.032 m.

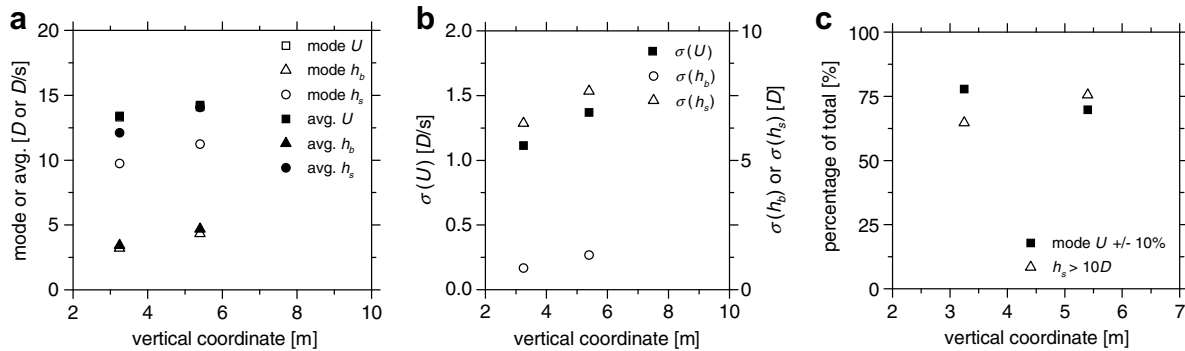


Fig. 10. Log-normal fit parameters (average, mode and standard deviation; a and b) and flow stability parameters (c) for experiments at 3.25 m and 5.40 m from the column base ($U_L \approx 0.099$ m/s, $U_G \approx 0.085$ m/s); column diameter: 0.032 m.

for bubble velocity, bubble length and liquid slug length are represented in Fig. 9. The statistical parameters of the log-normal fits (average, mode and standard deviation) and additional flow stability parameters are plotted in Fig. 10, against the vertical coordinate of the column. More details on the calculation of the parameters of the log-normal fits can be found in Campos Guimarães and Sarsfield Cabral (1997).

The analysis of the charts indicates that all depicted parameters increase along the column (the frequency distribution curves shift towards higher classes). Coalescence and expansion effects are accountable for the increase in the length of the liquid slugs and gas bubbles. As coalescence occurs along the column there is a decrease in the number of short liquid slugs and an increase in the number of long bubbles. This is further strengthened by the expansion effect, for the bubble length in particular.

The slight increase in bubble velocity along the column requires a more detailed analysis. Although one would expect a decrease due to less frequent coalescences and less intense interactions, a second effect must be taken into consideration: the gas-phase expansion. Indeed, the increase in the velocity due to the expansion of all bubbles flowing upstream (below) of each bubble overcomes the aforementioned decrease. Hence the overall slight increase of the average bubble velocity.

It is interesting to observe that the frequency distribution curves of all mentioned parameters become wider for higher vertical column position (a behaviour corroborated by the values of the standard deviation of the log-normal fits).

Two flow stability parameters were defined: the percentage of bubbles flowing after long slugs ($h_s > 10D$) and the percentage of bubbles whose velocity is within a 10% interval around the corresponding mode (most frequent value in a frequency distribution curve). The first parameter directly indicates the proportion of bubbles not undergoing coalescence (a direct indicator of flow stability) and the second is related to the dispersion of the bubble velocities around the corresponding mode (an indirect indicator of the bubble-to-bubble interaction). Fig. 10c indicates that, at 5.4 m from the column base, 76% of the bubbles flow after slugs longer than 10D (whereas a figure of 64% was obtained at 3.25 m from base). This variation indicates an increase in the stability of the flow. The percentage of bubbles within a 10% interval around the bubble velocity mode is almost identical in the two column positions.

5.4.1.2. Superficial liquid and gas velocity (U_L and U_G). Four experiments with increasing superficial liquid velocity are compared. The frequency distribution curves for the main flow parameters are plotted in Fig. 11. The average, mode and standard deviation of the log-normal fits, and the flow stability parameters, are plotted

against the superficial liquid velocity in Fig. 12a–c. These charts confirm that, as expected (Eq. (1)), the average velocity of the bubbles increases with superficial liquid velocity (Fig. 11a–d and Fig. 12a). Moreover, the average length of the bubbles and the length of the liquid slugs decrease slightly with increasing superficial liquid velocity.

Due to flow continuity, the increase in the superficial liquid velocity, while keeping a constant superficial gas velocity, induces shorter bubbles and/or longer liquid slugs, at the column inlet. Shorter bubbles at inlet suggest a negative-slope trend, for the average bubble length, at the column top. Longer liquid slugs at inlet point towards a positive-slope trend for the average length of the liquid slugs at the column top, as well as a less frequent coalescence along the column. According to the results, this latter consequence has a dominant effect. Indeed, the less frequent coalescence strengthens the inlet trend for the average length of the bubbles and inverts the inlet trend for the average length of the liquid slugs (intense coalescence induces longer bubbles separated by longer liquid slugs). Thus, at the top of the column, both the average bubble length and liquid slug length decrease slightly for increasing superficial liquid velocity.

For all the mentioned parameters there is a decrease of the standard deviation for increasing superficial liquid velocity (Fig. 11a–d, e–h, i–l; Fig. 12b). This decrease together with the increasing percentage of bubbles within a 10% interval around the velocity mode (Fig. 12c) indicates an increase of the flow stability for increasing superficial liquid velocity.

Data from four experiments with increasing superficial gas velocity are also compared in this section. The average, mode and standard deviation of the log-normal fits (of the frequency distribution curves) and the flow stability parameters are plotted against the superficial gas velocity in Fig. 12d–f. As shown in the charts, the average (and mode) of the velocity and length distributions increase with increasing superficial gas velocity (Fig. 12d). The average length of liquid slugs increases slightly with increasing superficial gas velocity (Fig. 12d), whereas the corresponding mode has an opposite behaviour. These latter variations are coherent with the increasing asymmetry of the corresponding frequency distribution curves.

Due to flow continuity, the increase of the superficial gas velocity, while keeping the superficial liquid velocity constant, induces longer bubbles and/or shorter liquid slugs, at the column inlet. Longer bubbles at inlet suggest a positive-slope trend for the average length of the bubbles, at the column top. Shorter liquid slugs at inlet point towards a negative-slope trend, for the average length of the liquid slugs, at the column top, as well as a more frequent coalescence along the column (as bubbles enter the column at shorter distances). The coalescence rate effect is once again domi-

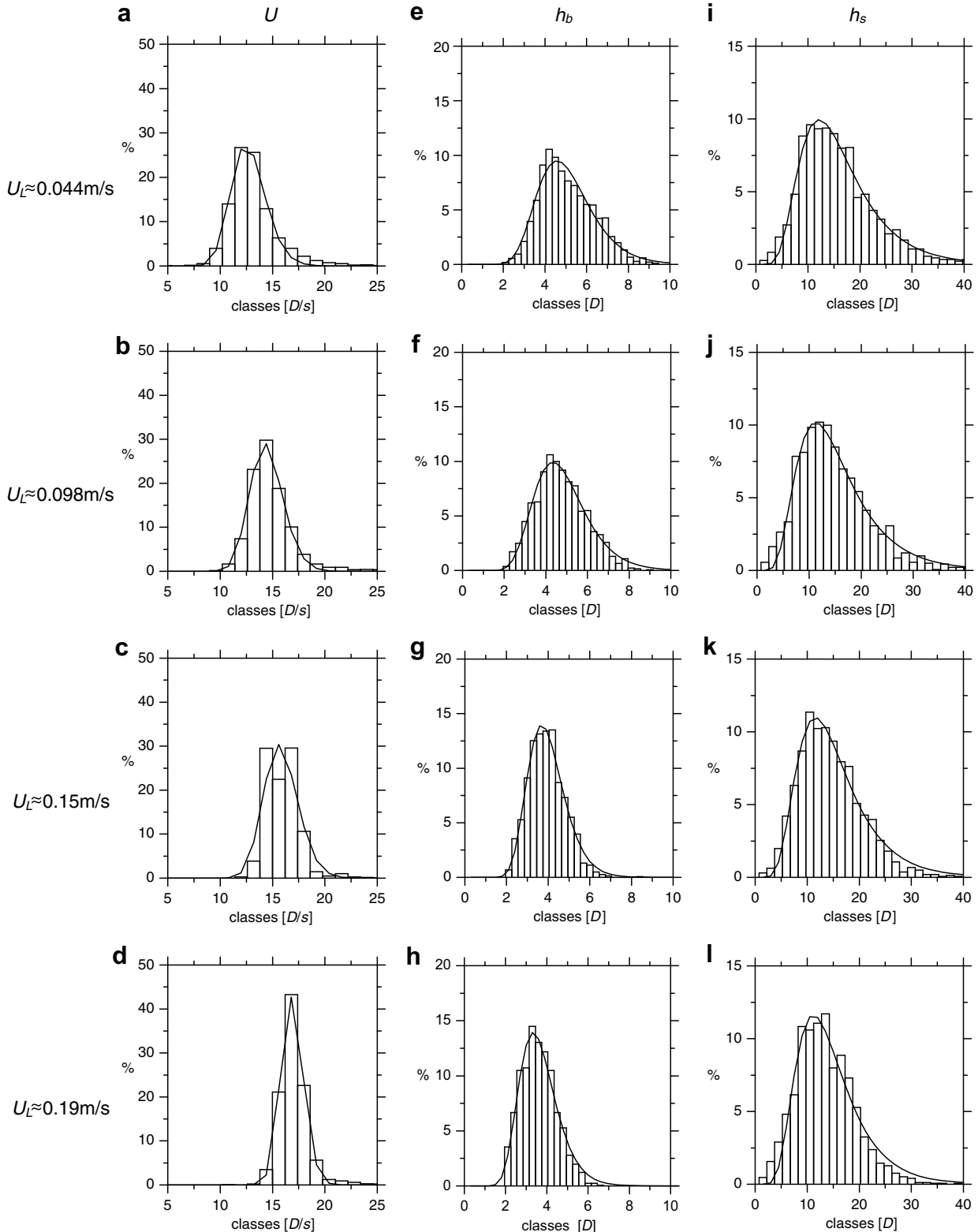


Fig. 11. Frequency distributions curves and log-normal fittings for experiments with $U_G \approx 0.085$ m/s and $U_L \approx 0.044, 0.098, 0.15$ and 0.19 m/s; vertical coordinate: 5.4 m; column diameter: 0.032 m.

nant in terms of the output distributions of bubble lengths and liquid slug lengths (as intense coalescence induces longer bubbles and longer liquid slugs). Indeed, these two flow parameters increase for increasing superficial gas velocity. Notice that the

slight decrease in the liquid slug length mode, for increasing superficial gas velocity (Fig. 12d), is a direct consequence of the increasing asymmetry of the corresponding frequency distribution curves.

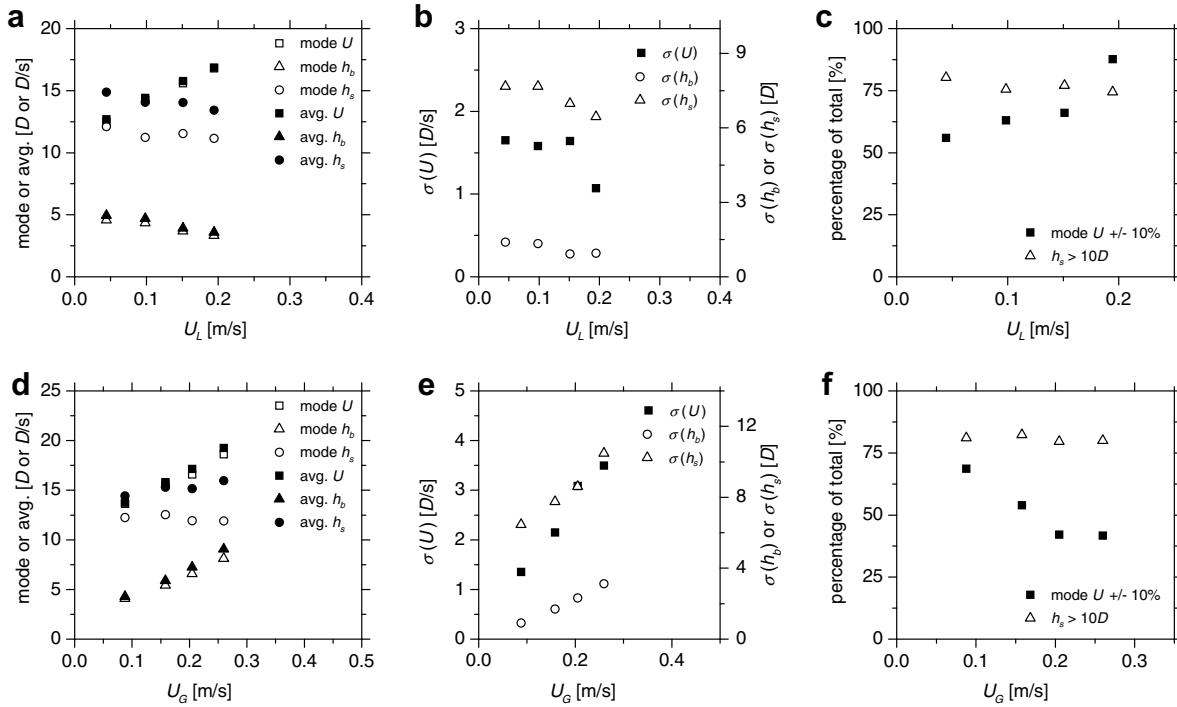


Fig. 12. Log-normal fit parameters (average, mode and standard deviation) and flow stability parameters for: (a), (b) and (c) experiments with $U_G \approx 0.085$ m/s and $U_L \approx 0.044$, 0.098, 0.15 and 0.19 m/s; (d), (e) and (f) experiments with $U_L \approx 0.10$ m/s and $U_G \approx 0.088$, 0.16, 0.21 and 0.26 m/s; vertical coordinate: 5.4 m; column diameter: 0.032 m.

The standard deviation of the frequency distribution curves escalates for increasing superficial gas velocity (Fig. 12e). This variation together with the decreasing percentage of bubbles within a 10% interval around the bubble velocity mode (Fig. 12f) indicates a less stabilized flow pattern for increasing superficial gas velocity.

5.4.2. Column II – 0.052 m ID

5.4.2.1. Superficial liquid and gas velocity (U_L and U_G). Four experiments with increasing superficial liquid velocity in a 0.052 m column are compared. The average, mode and standard deviation of the log-normal fits (of the frequency distribution curves) and the

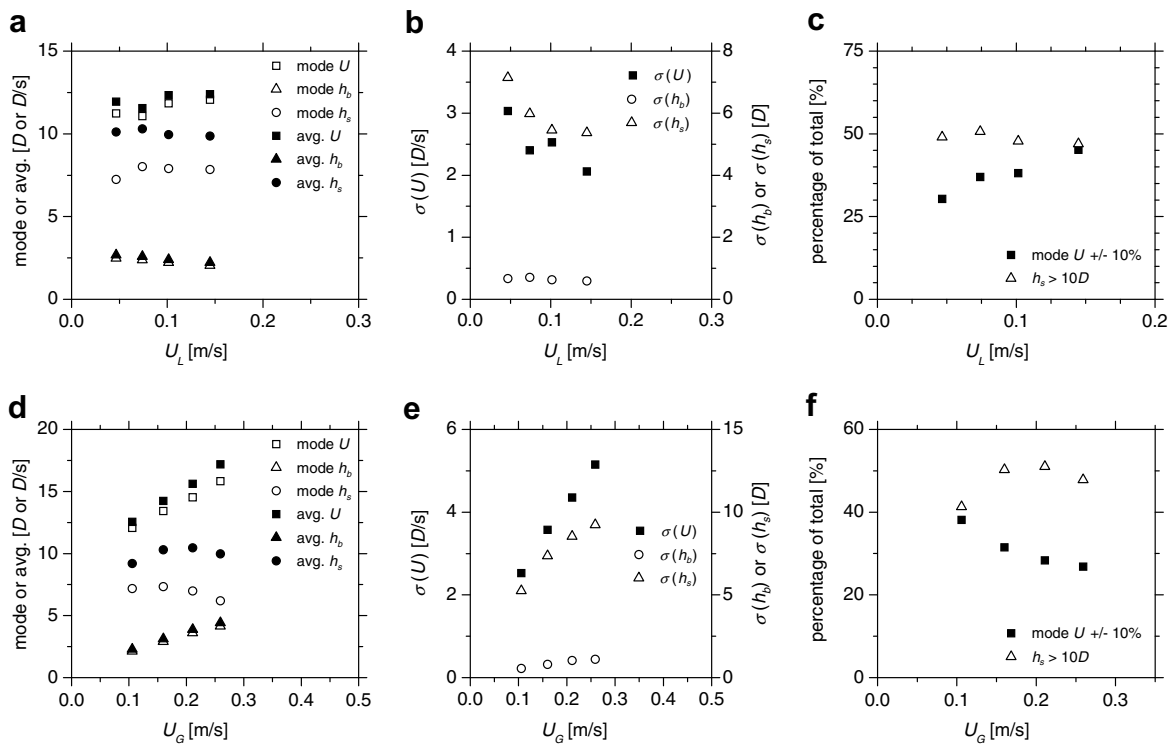


Fig. 13. Log-normal fit parameters (average, mode and standard deviation) and flow stability parameters for (a), (b) and (c) experiments with $U_G \approx 0.10$ m/s and $U_L \approx 0.047$, 0.074, 0.10 and 0.15 m/s; (d), (e) and (f) experiments with $U_L \approx 0.10$ m/s and $U_G \approx 0.11$, 0.16, 0.21 and 0.26 m/s; vertical coordinate: 5.4 m; column diameter: 0.052 m.

flow stability parameters are plotted against the superficial liquid velocity in Fig. 13a–c. As expected, the average (and mode) of the velocity distributions increases with increasing superficial liquid velocity (Fig. 13a). Moreover, the average length of the bubbles and liquid slugs decreases slightly with increasing superficial liquid velocity (Fig. 13a).

Following an approach similar to the one used for the narrower column, it is seen that, by flow continuity, the increasing superficial liquid velocity for constant gas velocity induces shorter bubbles and longer slugs at the column inlet, as well as a lower coalescence rate along the column. As for the narrower column,

the effect over the coalescence rate is dominant, since the average length of bubbles and liquid slugs decrease slightly for increasing superficial liquid velocity.

The standard deviations of bubble velocity and liquid slug length decrease for increasing superficial liquid velocity (Fig. 13b). This variation together with the increasing percentage of bubbles within a 10% interval around the velocity mode (Fig. 13c) indicates an increase in flow stability for increasing superficial liquid velocity. Similar conclusions were drawn for the 0.032 m column.

Data from four experiments with increasing superficial gas velocity are also compared in this section. The frequency distribu-

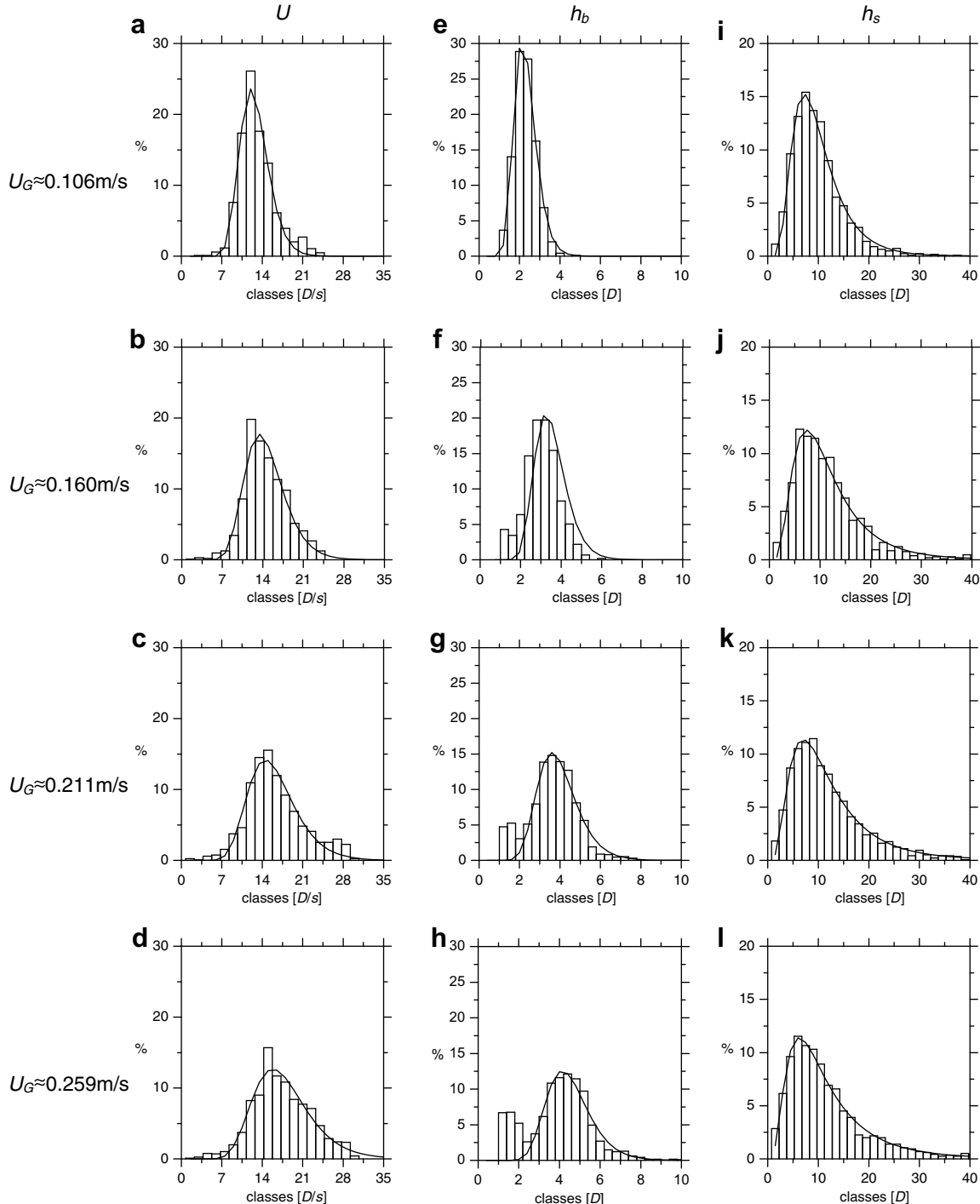


Fig. 14. Frequency distributions curves and log-normal fittings for experiments with $U_L \approx 0.10$ m/s and $U_G \approx 0.11, 0.16, 0.21$ and 0.26 m/s; vertical coordinate: 5.4 m; column diameter: 0.052 m.

tion curves for the main flow parameters are plotted in Fig. 14. The average, mode and standard deviation of the log-normal fits and the flow stability parameters are plotted against the superficial gas velocity in Fig. 13d–f. The average (and mode) of the velocity and length distributions increases for increasing superficial gas velocity (Fig. 14a–d, e–h and Fig. 13d). The average length of liquid slugs does not have a well-defined behaviour (Fig. 13d), whereas the corresponding mode slightly decreases. These latter variations are consistent with the increasing asymmetry of the corresponding frequency distribution curves (Fig. 14i–l).

As mentioned for the narrower column, the increasing superficial gas velocity for constant liquid velocity induces, by continuity, longer bubbles and shorter slugs at the column inlet, as well as higher coalescence rate along the column. In agreement with the conclusions drawn in the last section this behaviour points towards overall positive-slope trends at the column top for both the average length of bubbles and of liquid slugs. However, in Fig. 13d, an inconsistent variation can be observed in the average length of liquid slugs (in particular for the highest superficial gas velocity). This is the result of the competition between the effect of the length of the liquid slugs at the column inlet and the effect of coalescence along the column. For the reported experiment, this latter effect does not completely invert the initial trend.

It is interesting to note that a bimodal bubble length distribution seems to appear, mainly for higher values of superficial gas velocity (Fig. 14 g and h). Though very subtle, an identical behaviour has been observed for the narrower column. No phenomenological reasons can be given at this moment to account for these peculiar distributions.

The standard deviation of all frequency distribution curves escalates for increasing superficial gas velocity (Fig. 13e). This variation, together with the decreasing percentage of bubbles within a 10% interval around the bubble velocity mode (Fig. 13f), indicates a less stabilized flow pattern for increasing superficial gas velocity. Similar conclusions were drawn for the 0.032 m column.

A direct comparison between the above experimental results and other authors' findings (for instance Van Hout et al., 2001, 2002b) is not possible due to differences in the column diameters and in the superficial gas and liquid velocities. An alternative approach is followed. The reported experimental results together with Van Hout's data are used to support the development and validation of a slug flow simulator (Mayor et al., 2007a), with wide ranges of validity/applicability.

5.5. Experimental values of C and drift velocity

In order to evaluate the parameter C and the drift velocity (C and U_∞ as in Eq. (1)) for the experiments reported in the previous sections, the experimental average upward bubble velocities (U_B^{exp}) are plotted against the average superficial velocity of the mixture (U_M). This representation is shown in Fig. 15 for both column internal diameters (0.032 m and 0.052 m). These data are plotted together with the corresponding linear fit (for the 0.052 m column) and the theoretical predictions of U_B as given by Eq. (1), considering turbulent regime (C equal to 1.2). The values of U_B^{exp} were obtained directly from the measurements. The values of U_M were corrected to the pressure at coordinate 5.4 m (estimated using the knowledge of the void fraction inside the column, which was determined by comparing the liquid free-surface positioning before and after stopping the liquid and gas flows, at the end of the experiments).

A very good agreement is obtained between theoretical predictions and experimental results for the narrower column (0.032 m). Two experiments (open points) are slightly apart from the theoretical predictions, an expected behaviour since they refer to transi-

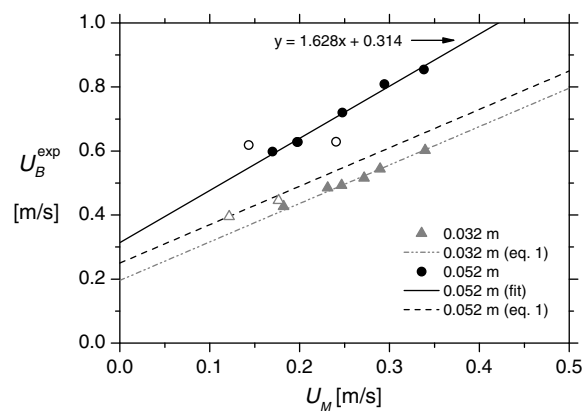


Fig. 15. Experimental average upward bubble velocity plotted against U_M for column internal diameters of 0.032 m and 0.052 m; vertical coordinate: 5.4 m.

tion (or quasi-transition) flow conditions in the main liquid (Re_{U_M} equal to 3890 and 5650, respectively, with U_M corrected for the pressure at 5.4 m).

The linear fit of the experimental data for the 0.052 m column did not take into consideration two experiments (open points) whose corresponding velocity values are, to some extent, apart from the trend. A very good correlation is achieved for the remaining data.

A poor agreement is observed between theoretical predictions and experimental results for the larger diameter column (0.052 m), a result already reported by other researchers (Van Hout et al., 2001, 2002b, among others). Both the experimental parameter C (1.628) and the experimental drift velocity U_∞ (0.314 m/s) are moderately higher than the theoretical predictions for turbulent regime ($C = 1.2$ and $U_\infty = 0.25$ m/s; for a 0.052 m column). This discrepancy must be ascribed to the following. First, the highly aerated liquid slugs (in particular for high superficial gas velocities) can result in an increase in the experimental drift velocity (Van Hout et al., 2002b). Secondly, the level of turbulence in the liquid between bubbles (higher than for the narrower column, as confirmed by the Reynolds numbers in Table 2), generates instantaneous velocity profiles considerably different from the average ones. The trailing bubble nose sways away from the tube axis, following the fastest portion of fluid ahead, which results in continuous elongations and relaxations of the bubble shape (easily observed in the video frames), even when no Taylor bubbles are ahead. The high values of experimental parameter C are consistent with this scenario. However, and as suggested by Shemer et al. (2007), it is also possible that some residual oscillations in the liquid, related to a slow decay of the leading bubble wake perturbation, may also contribute to the observed high values of parameter C . Further studies are required in order to clarify this issue.

6. Conclusions

An experimental study on free-bubbling gas–liquid vertical slug flow is reported. Data were acquired through a non-intrusive image analysis technique, based on the straightforward analysis of sequences of image frames of the flow. The flow pattern in the wake of the bubbles and in the liquid was turbulent.

Parameters such as the column diameter, the column vertical coordinate, the superficial liquid and gas velocities and the velocity and the length of the leading bubble were found not to influence the bubble-to-bubble interaction curve. A single correlation for the bubble-to-bubble interaction is proposed, relating the trailing bubble velocity to the length of the liquid slug ahead of the bubble.

Bubble-to-bubble interaction was found to occur only for liquid slugs shorter than 8–10D.

As expected, the increasing superficial liquid velocity was shown to enhance the flow stability, for both column diameters. The superficial gas velocity produced the opposite effect. Considerable asymmetry has been observed for both column diameters in the distributions of the liquid slug lengths.

A good agreement was found between theoretical predictions for U_B and the experimental results obtained for the 0.032 m internal diameter column. For the 0.052 m internal diameter column, however, the theory under-predicted the experimental results considerably, a discrepancy also reported by other researchers (Van Hout et al., 2001, 2002b, among others).

The obtained bubble-to-bubble interaction curve, the frequency distribution curves of the main flow parameters and the corresponding average values are crucial data for the development and validation of slug flow simulators with wide ranges of validity/applicability.

Acknowledgments

The authors gratefully acknowledge the financial support of Fundação para Ciência e Tecnologia through project POCI/EQU/33761/1999 and scholarship SFRH/BD/11105/2002. POCI (FEDER) also supported this work via CEFT.

Appendix Results. of error analysis for main flow parameters

Every measurement is accomplished within the precision and bias limits of the equipment used in the experimental procedure. Considering that every measured quantity has an associated uncertainty, it is interesting to assess how these uncertainties propagate through the algebraic transformations required to compute every dependent variables. Following the *general uncertainty analysis approach*, a procedure has been implemented for parameters such as bubble velocity, bubble length and liquid slug length, gas and superficial liquid velocities and experimental upward bubble velocity, in order to calculate their relative uncertainties due to initial uncertainties in the definition of, for instance, the positioning of the bubble boundaries. The results of this analysis are shown in Table 3 (More details on this approach can be found in Mayor et al., 2007b).

The results indicate that every slug cell parameter (bubble velocity, bubble length and liquid slug length), determined through the reported image analysis technique, is calculated with a relative uncertainty lower than 7.0%. The experimental upward bubble velocity is assessed with a 5.0% uncertainty. Additionally, the superficial gas and liquid velocities are evaluated with relative uncertainties between 6.3% and 7.5%. These low relative uncertainties increase the level of confidence in the reported results.

The aforementioned results refer to the uncertainty of individual bubbles. Shorter intervals (in percentage) are found, however, if one assesses the intervals around the sample averages that contain, with a certain confidence level, the real average of each parameter (i.e. the confidence intervals: $\pm tS_x/\sqrt{n}$). To illustrate

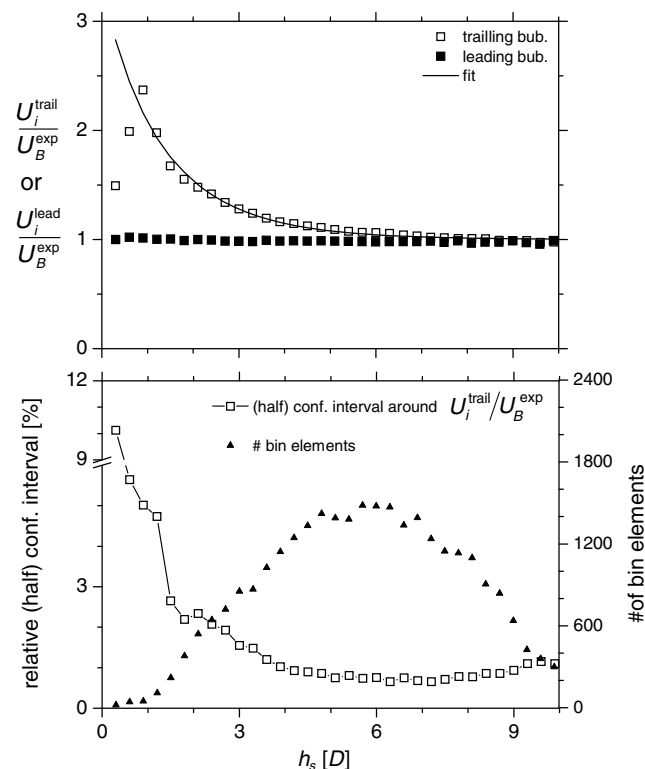


Fig. 16. Relative (half) confidence intervals for the estimates of $U_i^{\text{trail}}/U_B^{\text{exp}}$ and number of elements in each slug length class (bin) plotted against h_s ; confidence intervals computed as $\pm tS_x/\sqrt{n}$, for confidence level 95%; 0.032 m ID.

the aforesaid, the relative (half) confidence intervals around the trailing bubble velocity estimates of Fig. 8b, are given, in Fig. 16, together with the number of elements in each slug length class. This representation shows that, for liquid slugs longer than 4D, the half confidence interval extends no further than 1.1% from the corresponding average, which confirms the accurateness of the experimental technique and reported results.

References

- Aladjem Talvy, C., Shemer, L., Barnea, D., 2000. On the interaction between two consecutive elongated bubbles in a vertical pipe. *Int. J. Multiphase Flow* 26, 1905–1923.
- Campos Guimarães, R., A. Sarsfield Cabral, J. (1997). *Estatística*, McGraw-Hill de Portugal Limitada.
- Collins, R., De Moraes, F.F., Davidson, J.F., Harrison, D., 1978. The motion of large gas bubble rising through liquid flowing in a tube. *J. Fluid Mech.* 28, 97–112.
- Mayor, T.S., Pinto, A.M.F.R., Campos, J.B.L.M., 2007a. Hydrodynamics of gas-liquid slug flow along vertical pipes in turbulent regime. A simulation study. *Chem. Eng. Res. Des.* 85 (A11), 1–17.
- Mayor, T.S., Pinto, A.M.F.R., Campos, J.B.L.M., 2007b. An image analysis technique for the study of gas-liquid slug flow along vertical pipes - Associated uncertainty. *Flow Meas. Inst.* 18 (3–4), 139–147.
- Mayor, T.S., Pinto, A.M.F.R., Campos, J.B.L.M., 2008. On the gas expansion and gas hold-up in vertical slugging columns - a simulation study. *Chem. Eng. Process.* 47, 799–815.
- Moissis, R., Griffith, P., 1962. Entrance effects in a two-phase slug flow. *J. Heat Transfer* 84, 29–39.
- Nicklin, D.J., Wilkes, J.O., Davidson, J.F., 1962. Two-phase flow in vertical tubes. *Trans. Institut. Chem. Eng.* 40, 61–68.
- Nogueira, S., Sousa, R.G., Pinto, A.M.F.R., Riethmüller, M.L., Campos, B.L.M., 2003. Simultaneous PIV and pulsed shadow technique in slug flow: a solution for optical problems. *Exp. Fluids* 35, 598–609.
- Nogueira, S., Riethmüller, M.L., Campos, B.L.M., Pinto, A.M.F.R., 2006. Flow patterns in the wake of a Taylor bubble rising through vertical columns of stagnant and flowing Newtonian liquids: an experimental study. *Chem. Eng. Sci.* 61, 7199–7212.
- Pinto, A.M.F.R., Campos, J.B.L.M., 1996. Coalescence of two gas slugs rising in a vertical column of liquid. *Chem. Eng. Sci.* 51 (1), 45–54.
- Pinto, A.M.F.R., Pinheiro, M.N.C., Campos, J.B.L.M., 1998. Coalescence of two gas slugs rising in a co-current flowing liquid in vertical tubes. *Chem. Eng. Sci.* 53 (16), 2973–2983.

Table 3

Relative uncertainties of some flow parameters

	Relative uncertainty [%]
U_i	5.0
$h_{b,i}$	2.5
$h_{s,i}$	7.0
U_L	6.3
U_G	7.5
U_B^{exp}	5.0

Shemer, L., Gulitski, A., Barnea, D., 2007. Movement of two consecutive Taylor bubbles in vertical pipes. *Multiphase Sci. Technol.* 19 (2), 99–120.

Sotiriadis, A.A., Thorpe, R.B., 2005. Liquid re-circulation in turbulent vertical pipe flow behind a cylindrical bluff body and a ventilated cavity attached to a sparger. *Chem. Eng. Sci.* 60 (4), 981–994.

The MathWorks, Inc., 2002. Help Files of MATLAB: The Language of Technical Computing.

Van Hout, R., Barnea, D., Shemer, L., 2001. Evolution of statistical parameters of gas–liquid slug flow along vertical pipes. *Int. J. Multiphase Flow* 27 (9), 1579–1602.

Van Hout, R., Gulitski, A., Barnea, D., Shemer, L., 2002a. Experimental investigation of the velocity field induced by a Taylor bubble rising in stagnant water. *Int. J. Multiphase Flow* 28 (4), 579–596.

Van Hout, R., Barnea, D., Shemer, L., 2002b. Translational velocities of elongated bubbles in continuous slug flow. *Int. J. Multiphase Flow* 28 (8), 1333–1350.

White, E.T., Beardmore, R.H., 1962. The velocity of single cylindrical air bubbles through liquids contained in vertical tubes. *Chem. Eng. Sci.* 17, 351–361.